Polarization Conversion from a Two-Port Impedance Loaded Tag

Luis Felipe Fonseca Dias, Camille Jouvaud, Christophe Delaveaud, Hervé Aubert

Polarization Conversion from a Two-Port Impedance Loaded Tag

Luis Felipe Fonseca Dias*†, Camille Jouvaud*, Christophe Delaveaud*, Herve Aubert†
*Univ. Grenoble Alpes, CEA, Leti, 38054 Grenoble, France
{luisfelipe.fonsecadias, camille.jouvaud, christophe.delaveaud}@cea.fr
†Univ. Toulouse, CNRS, LAAS (Laboratoire d'Analyse et d'Architecture des Systèmes), 31031 Toulouse, France,
herve.aubert@toulouse-inp.fr

***Abstract*—The electromagnetic clutter mitigation is increasingly demanded for achieving the indoor identification and long-range reading of wireless and passive sensor tags. In this paper, a new Polarization Diversity scheme is proposed to reduce the clutter and potentially, to increase the reader to tag separation distance. The proposed wireless tag is a two-port patch antenna loaded by proper passive impedances. When illuminated by a circularly polarized electromagnetic field, the proposed tag backscatters a linearly or circularly polarized field, depending on the choice of four passive load impedances. This polarization conversion is then easily controlled, and can be advantageously implemented to improve the existing wireless systems by reducing the line-of-sight environment clutter and, from this, increasing reader-to-tag separation distance.**

***Index Terms*—electromagnetic backscattering, passive scatterer, polarization conversion, polarization diversity.**

I. Introduction

The advent of 5G has solidified the notion of Internet of Things and the increase of the number of wireless sensors sharing a common space. As consequence, mitigating the electromagnetic clutter is necessary to achieve long-range detection and reading of such sensors, such as RFID sensor tags or so-called *antenna sensors* [1].

Techniques for remotely and wirelessly interrogating passive sensors or tags can be mainly divided into two classes: In the first class, the *frequency* of the electromagnetic field backscattered by the sensor differs from the frequency of the incident field [2]. Still in this line, another well-known technique is based on the frequency hopping, in which the frequency used in the wireless link is outright shifted [3], [4]. In the second class, the *polarization* of the electromagnetic field backscattered by the sensor differs from the polarization of incident field. For instance, Circular-to-Circular Polarization (CP-to-CP) conversion can be used for increasing by over 17% the reading range (i.e., the separation distance between the reader and the sensor) compared with the well-known Linear-to-Linear Polarization (LP-to-LP) conversion [5]. The use of Vertical-to-Horizontal (V-to-H) or Horizontal-to-Vertical (H-to-V) polarization conversion allows reaching reading ranges exceeding 50 m [6], and the use of CP antennas for wireless indoor communication provides better overall performance by mitigating the electromagnetic clutter in indoor applications [7], notably for line-of-sight channels, which offer better cross-polarization discrimination. Recent works proposed to use depolarizing tags to compensate misalignment issues between tag and reader [8] and even exploit the misalignment to their advantage [9]. However, no practical solutions based on the polarization diversity and using impedance loaded tags have been reported to date. Recently, the Authors proposed a new technique [10] based on the control of the polarization of the electromagnetic field backscattered by passive *single-port* antennas. The proof-of-concept was established only from theoretical considerations and illustrated from preliminary simulation results. In the present study, the technique is extended to *two-port* antennas in order to achieve four different polarizations of the backscattered field from an incident circularly-polarized electromagnetic field. Measurement results obtained from a loaded two-port microstrip patch antenna acting as a tag (or a passive scatterer) are provided for experimental validation purpose.

The paper is organized as follows. Section II describes the two-port patch antenna and passive impedances connected to the two input ports of the antenna. Section III details the experimental setup and the calibration process applied for measuring the Radar Cross Section (RCS) of the tag. Section IV reports the experimental validation of the proposed control of the polarization of the electromagnetic field backscattered by the tag. Finally, conclusions and perspective outlines are provided in Section V.

II. Two-Port Impedance Loaded Tag

A. Two-Port Patch Antenna

The proposed antenna geometry of the tag is shown in Fig. 1. The tag is a microstrip patch antenna on a combination of two types of substrates: FR-4 and air, with ε_r equal to 4.3 and 1, respectively, designed to operate at 2.45 GHz. The patch itself is a thin copper square (0.37λ x 0.37λ surface, 35 μm thickness) cut from a bigger square copper board (0.65λ x 0.65λ x 0.007λ). The ground plane is a copper board with the same dimensions as the first board. As illustrated in Fig. 1b, the two copper boards are superposed and held apart by nylon (ε_r = 3.5) spacers, creating an air gap of thickness t_{air}. Both conducting faces are directed outwards. The antenna's ports are physically implemented by two transversal feeding probes, positioned at the points x_f and y_f (see Fig. 1a).

Antenna measurements are performed in an anechoic chamber, and the full-wave electromagnetic simulations are exe-

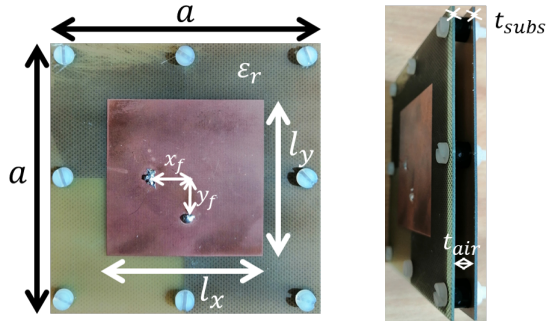

(a) (b)

Fig. 1. The two-port microstrip patch antenna operating at 2.45 GHz: (a) front view and (b) side view. Location of the two ports are given by x_f and y_f, respectively (a = 0.65λ, $l_y = l_x = 0.37\lambda$, $x_f = y_f = 0.09\lambda$, $t_{air} = 0.04\lambda$, $t_{subs} = 0.007\lambda$ and $\varepsilon_r = 4.3$, where $\lambda = 122.4$ mm).

cuted by the 3D simulation suite MWS CST. It can be observed in Fig. 2 that the simulated input reflection coefficients at the two input ports are in very good agreement with the measured ones. A good impedance matching is achieved over the bandwidth of 5% of the operating frequency (2.45 GHz). As shown in Fig. 3, an excellent agreement is obtained between the simulated and measured co-polar antenna gain when both input ports are separately fed (when one port is excited, the other port is loaded by a 50 Ω impedance). The broadside gain is about 8 dBi at 2.45 GHz.

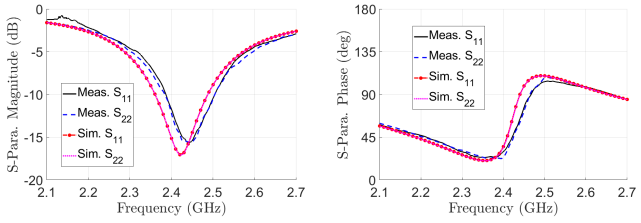

(a) (b)

Fig. 2. Measured and simulated scattering parameters S_{11} and S_{22} at the two input ports 1 and 2 of the microstrip antenna shown in Fig. 1: (a) Magnitude (in dB) and (b) Phase (in degrees).

B. Passive Two-Port Circuit for loading the Antenna

The structural scattering is mostly dependent on the geometry of the antenna, and for this reason, a Coplanar Transmission Line (CPTL) is used as the two-port circuit of the scatterer under study. The transmission line consists of a central conductor, of length l_{cp} and width w_{ser}, separated on both sides by a narrow air gap (g) from the antenna ground. The width w_{ser} has been designed so that the line's resistance coincides with the reference impedance Z_0 = 50 Ω.

For the load circuits, we propose two setups adding lumped resistances on the transmission line. The first configuration will be called the "series" setup, illustrated in Fig. 4b. This setup consists of replacing a part of the central conductor to a lumped resistance, represented as a red box and labeled as

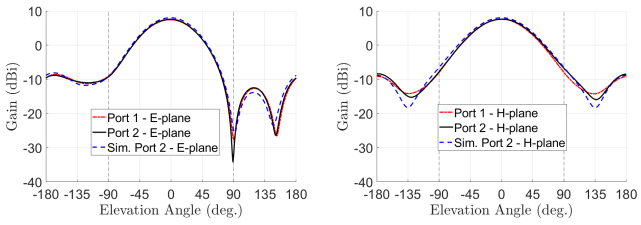

(a) (b)

Fig. 3. Measured and simulated co-polar gain at 2.44 GHz in (a) the E-plane and (b) H-plane (dashed blue : MWS CST simulation results; dash-dotted red : measured gain when port 1 is excited and port 2 is loaded by a 50 Ω impedance, and the solid black: the measured gain when port 2 is excited and port 1 is loaded by a 50 Ω impedance.

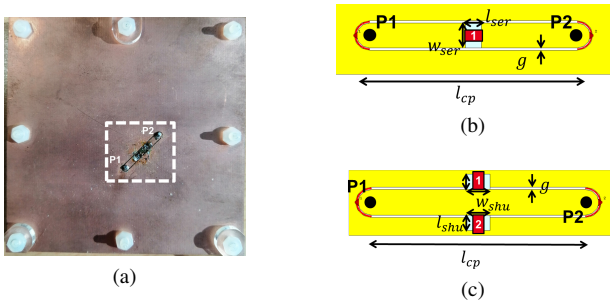

(a) (b) (c)

Fig. 4. (a) Back view of the realized two-port patch antenna with CPTL connecting ports 1 and 2 (P1 and P2), integrated on the antenna ground. The "series" circuit setup, is highlighted by the dashed white box. Coplanar Transmission Lines' representations on the back view of the patch antenna (zoomed in) from MWS CST with (b) "series" setup with the resistance position as the red box labeled 1 and (c) "parallel" setup with the resistances positions as the red boxes labeled 1 and 2. $l_{cp} = 15.7$ mm, $l_{ser} = 1.2$ mm, $w_{ser} = 2$ mm, $l_{shu} = 1.2$ mm, $w_{shu} = 1.7$ mm and $g = 0.18$ mm.

resistance 1 in Fig. 4b. The second setup, which will be called as the "parallel" setup, consists of a balanced bridge between central conductor and ground using equal lumped resistances. Both resistances are indicated as red boxes, labelled as *resistance 1* and *resistance 2*, as shown in Fig. 4c. In both setups, the lumped elements are positioned in the middle of the line, or at l_{cp}/2. Fig. 4a displays the back view of a realized two-port patch scatterer with the "series" line setup highlighted.

III. Experimental Setup for the RCS Measurements

In this section, we describe the experimental setup used to charactere the electromagnetic backscattering of the tag, and we briefly describe calibration process used for measuring the backscattered field of the tag.

The polarization conversion achieved by the tag, loaded by proper passive impedances (see Section IV), is validated here from measurement results obtained in an anechoic chamber. Identical transmitting (Tx) and receiving (Rx) horn antennas (about 10 dBi of gain in the frequency band of interest) are used for the measurements. The experimental configuration is bistatic, as the Tx- and Rx-antennas are not co-located. The Tx-antenna is vertically polarized, while the orientation of the Rx-antenna is mechanically controlled to measure the

backscattered electromagnetic field for different polarization modes. We derive the so-called *measured backscattering matrix* $[S^m]$ (see [11]) from these results. The tag is called in this Section the Scatterer Under Test (SUT). SUT, Tx- and Rx-antennas are placed half-height up the anechoic chamber. The separation distance between the Tx- and Rx-antennas is 0.7 m (5.7λ), while the distance between these two antennas and SUT is 3.35 m (far-field condition). Moreover, the electromagnetic field transmitted by the Tx-antenna is normally incident upon the SUT planar surface, and the bistatic angle is 11°. The SUT backing is composed of a fixed plastic base to monitor the azimuth angle of the scatterer, and is placed on a foam support, as shown in Fig. 5. A rotating plastic hollow disk is used to hold the antenna and to control the relative incident field polarization to measure the backscattering matrix $[S^m]$. The experimental setup offers a tunable measurement bandwidth from 1.5 GHz to 6 GHz, with the frequency step of 1 MHz. The setup is calibrated from *Single-Reference Calibration* (SRC) technique proposed in [11], and adapted to our need (bistatic configuration) [12]. The goal of this calibration step is to derive the so-called *calibrated backscattering matrix* $[S^c]$ by compensating the eventual distortion due to the electromagnetic propagation on the measured backscattering matrix $[S^m]$ [13]. The SRC technique is preferred here to the standard calibration process (see, e.g., [14]) because it is more time-efficient, while ensuring the similar measurement accuracy of RCS.

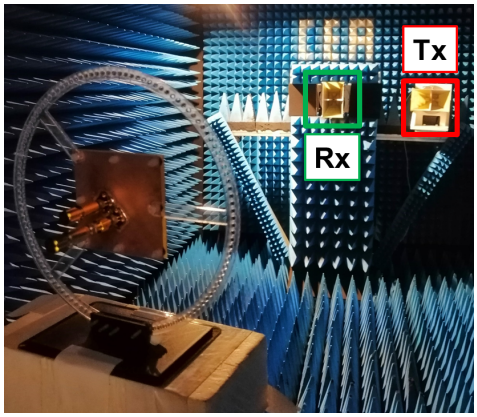

Fig. 5. Experimental setup in the anechoic chamber with identical horn (Tx- and Rx-) antennas and the tag (SUT) placed on the plastic hollow disk over a foam support.

IV. Polarization Conversion from Impedance Loading of the Tag

In this section, we show that it is possible to control the polarization of the electromagnetic field backscattered by the impedance loaded tag of Section II, when the tag is illuminated by a circularly polarized field. The impedance loads have been determined from the extension to two-port antennas of the electromagnetic analysis reported by the Authors in [10] for modeling single-port antennas. To achieve the Left-Handed-to-Right-Handed Circular Polarization (LHCP-to-RHCP) conversion, "parallel" *resistance 1* and *resistance 2*, defined in Subsection II-B, are both equal to 0 Ω (jumpers). To achieve the LHCP-to-LHCP conversion, "series" *resistance 1* is equal to 20 Ω. To obtain the first CP-to-LP conversion, "parallel" *resistance 1* and *resistance 2* are both equal to 56 Ω and finally, to achieve the second CP-to-LP conversion, the resistance load of the "series" *resistance 1* is equal to 120 Ω.

The results reported in this Section are derived from the calibrated backscattering matrix $[S^c]$, when the tag is illuminated by a LHCP electromagnetic field. The Axial Ratio [15] of the field backscattered by the tag is measured to determine the polarization (linear, elliptical or circular) of this field. When the backscattered field is circularly polarized at the measured operating frequency (2.46 GHz), the phase difference between the vertical and horizontal components of this field is measured in order to discriminate between Left-Handed (90°) and Right-Handed (−90° or 270°) circular polarizations. When the backscattered field is linearly polarized, the magnitude of the co- and cross-polarized components indicates the polarization isolation of each LP state.

A. LHCP-to-RHCP Conversion

The LHCP-to-RHCP conversion is achieved by soldering jumpers (0 Ω resistances) to connect the two sides of the ground to the central conductor, in the setup defined as "parallel", see Fig. 4c.

Fig. 6 shows stable Axial Ratio over the frequency band, which indicates that the metallic plate (generating the structural backscattering mode) has a predominant influence in the polarization of the backscattered electromagnetic field. The measured operating frequency (2.46 GHz) of the tag is very close to the resonant frequency of the patch antenna and consequently, the Axial Ratio reaches its highest value. Moreover, the phase difference (see Fig. 6) does not vary with frequency and is very close to 270° at 2.46 GHz. As expected, the electromagnetic field backscattered by the tag is then right-handed circularly polarized.

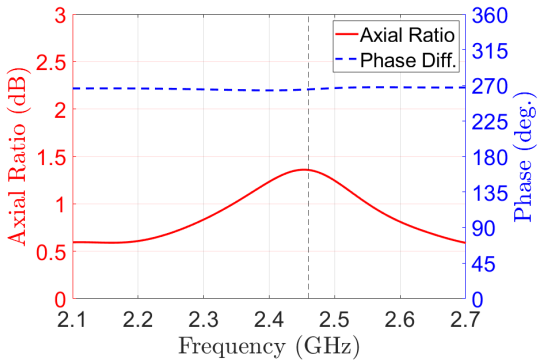

Fig. 6. Measured axial ratio of the electromagnetic field backscattered by the tag as a function of frequency (solid red) and Phase difference between vertical and horizontal components of this field as a function of frequency (dashed blue). The vertical dashed black line indicates the operating frequency (f_0 = 2.46 GHz). These measurement results are obtained from jumper connections (0 Ω resistances) to the modified CPTL, the "parallel" setup.

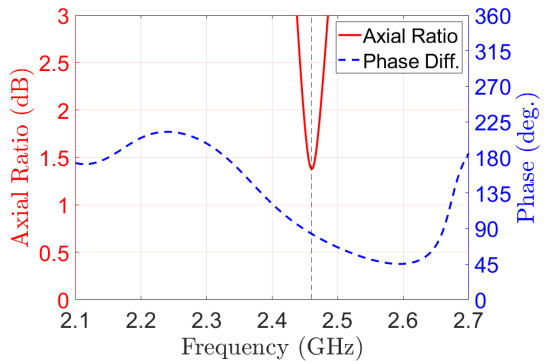

Fig. 7. Measured axial ratio of the electromagnetic field backscattered by the tag as a function of frequency (solid red) and Phase difference between vertical and horizontal components of this field as a function of frequency (dashed blue). The vertical dashed black line indicates the operating frequency (f_0 = 2.46 GHz). These measurement results are obtained from connecting a resistance R = 20 Ω to the modified CPTL, "series" setup.

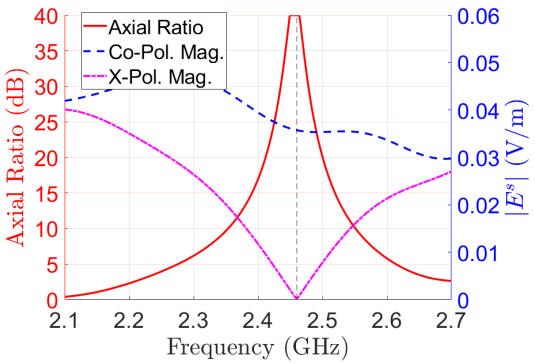

Fig. 8. Measured axial ratio of the electromagnetic field backscattered by the tag as a function of frequency (solid red) and magnitudes of orthogonal modes' components of this field as a function of frequency: $-60°$ slanted co-polar (dashed blue) and its cross-polar magnitude (dash-dotted magenta). The vertical dashed black line indicates the operating frequency (f_0 = 2.46 GHz). These measurement results are obtained from connecting resistances equal to 56 Ω to the modified CPTL, the "parallel" setup.

B. LHCP-to-LHCP Conversion

We achieve here the CP-to-CP conversion from using a passive impedance load able to affect significantly the backscattered electromagnetic field backscattered by the tag, and to generate left-handed circularly polarized backscattered field. A lumped resistance R = 20 Ω is used in the "series" circuit setup, as illustrated in Fig. 4b.

From Fig. 7, we can observe a narrow-band response (about 2%) in which the required polarization is achieved. At the operating frequency, the Axial Ratio reaches its minimum value ($<$ 1.4 dB). Fig. 7 displays the measured phase difference between vertical and horizontal components of the electromagnetic field backscattered by the tag as a function of frequency. The phase difference is of $83°$ (very close to $90°$) at the operating frequency and consequently, the field backscattered by the tag is left-handed circularly-polarized, as expected.

C. LHCP-to-LP Conversion ($-60°$ slant)

The third polarization conversion is the CP-to-LP conversion, or a $-60°$ slanted LP response. In this case, we have two lumped resistances bridging the central conductor to the antenna's ground, in the "parallel" circuit setup. The values of the two resistances are R = 56 Ω.

Fig. 8 displays the measured Axial Ratio of the electromagnetic field backscattered by the tag. It exceeds 40 dB and consequently, ensures a good polarization isolation. The A circular polarization is achieved at frequencies outside the bandwidth of interest, since teh Axial Ratio is lower than 3 dB below 2.22 GHz and above 2.67 GHz. As expected, we observe from Fig. 8 that the measured magnitude of the cross-polar component ($30°$ slant) reaches its minimum value at the operating frequency (2.46 GHz). From this measurement result, we conclude that the field backscattered by the tag at the operating frequency is purely linearly polarized, and the polarization inclined of $-60°$ from the original Vertical and Horizontal base.

D. LHCP-to-LP Conversion ($9°$ slant)

For the final polarization conversion, the impedance load of the tag leads to another LP backscattered electromagnetic field, with a slant angle lower than $9°$. This is implemented using the "series" circuit setup with a lumped resistance equal to R = 120 Ω.

The resulting Axial Ratio of the electromagnetic field backscattered by the tag is found higher than 25 dB, leading to a good isolation, as shown in Fig. 9. Moreover, it can be observed that the cross-polar component ($99°$ slant) reaches its minimum also at the operating frequency (2.46 GHz). However, the cross-polarized component of the backscattered electromagnetic field is not zero and the polarization is inclined by $9°$ from the original Vertical and Horizontal base.

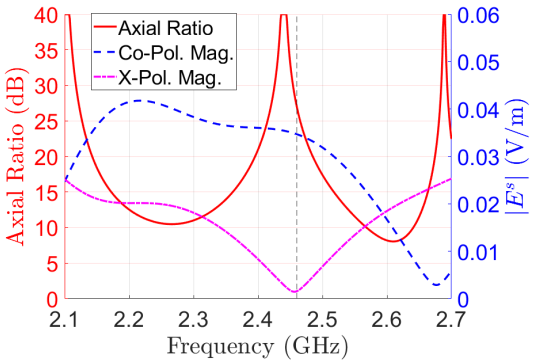

Fig. 9. Measured axial ratio of the electromagnetic field backscattered by the tag as a function of frequency (solid red) and magnitudes of orthogonal modes' components of this field as a function of frequency: $9°$ slanted co-polar (dashed blue) and its cross-polar magnitude (dash-dotted magenta). The vertical dashed black line indicates the operating frequency (f_0 = 2.46 GHz). These measurement results are obtained from connecting a resistance R = 120 Ω to the modified CPTL, "series" setup.

V. Conclusion

In this study, an impedance loaded patch antenna acting as a passive tag is presented, which can achieve four different polarization of the backscattered electromagnetic field (namely LHCP, RHCP and two slanted LP), when illuminated by a circularly-polarized electromagnetic field. Only four different resistance values are required to control the backscattered field polarization. Experimental results confirm the low axial ratio (less than 1.5 dB) predicted by a backscattering model and full-wave electromagnetic simulations in case of circularly-polarized (RH or LH) backscattered fields, and the excellent isolation (25 dB) in case of ($-60°$ and $9°$ slanted) linearly-polarized backscattered fields. The proposed technique based on polarization conversion from impedance loaded two-port tag may solve propagation issues faced in indoor applications of wireless sensor networks, specially when clutter presents minor levels of depolarization. This solution may be implemented without the need of battery or power supply, when considering passive tags. Moreover, LHCP-to-LHCP conversion can be advantageously applied to mitigate the impact of the electromagnetic clutter in a wireless link and potentially, increase the reader-to-tag separation distance in cluttered environments.

Acknowledgment

The Authors gratefully acknowledge the technical support on the measurements' setup of this work by Ph.D M. Caillet. The authors are also thankful for the insightful discussions with Ph.D S. Bories on backscattering studies.

References

[1] B. Paul, A. R. Chiriyath, and D. W. Bliss, "Survey of RF Communications and Sensing Convergence Research," *IEEE Access*, vol. 5, pp. 252–270, 2017.

[2] P. Pons, H. Aubert, P. Menini, and M. Tentzeris, "Electromagnetic Transduction for Wireless Passive Sensors," *Procedia Engineering*, vol. 47, pp. 1474–1483, Jan. 2012.

[3] S. Sabesan, M. J. Crisp, R. V. Penty, and I. H. White, "Wide Area Passive UHF RFID System Using Antenna Diversity Combined With Phase and Frequency Hopping," *IEEE Transactions on Antennas and Propagation*, vol. 62, no. 2, pp. 878–888, Feb. 2014.

[4] L. Zhu, M. Farhat, Y.-C. Chen, K. N. Salama, and P.-Y. Chen, "A Compact, Passive Frequency-Hopping Harmonic Sensor Based on a Microfluidic Reconfigurable Dual-Band Antenna," *IEEE Sensors Journal*, vol. 20, no. 21, pp. 12 495–12 503, Nov. 2020.

[5] J. García, A. Arriola, F. Casado, X. Chen, J. I. Sancho, and D. Valderas, "Coverage and read range comparison of linearly and circularly polarised radio frequency identification ultra-high frequency tag antennas," *IET Microwaves, Antennas & Propagation*, vol. 6, no. 9, pp. 1070–1078, Jun. 2012.

[6] D. Henry, J. G. D. Hester, H. Aubert, P. Pons, and M. M. Tentzeris, "Long-Range Wireless Interrogation of Passive Humidity Sensors Using Van-Atta Cross-Polarization Effect and Different Beam Scanning Techniques," *IEEE Transactions on Microwave Theory and Techniques*, vol. 65, no. 12, pp. 5345–5354, Dec. 2017.

[7] T. Rappaport and D. Hawbaker, "Wide-band microwave propagation parameters using circular and linear polarized antennas for indoor wireless channels," *IEEE Transactions on Communications*, vol. 40, no. 2, pp. 240–245, Feb. 1992.

[8] F. Costa, S. Genovesi, and A. Monorchio, "Chipless RFIDs for Metallic Objects by Using Cross Polarization Encoding," *IEEE Transactions on Antennas and Propagation*, vol. 62, no. 8, pp. 4402–4407, Aug. 2014.

[9] A. Vena, E. Perret, and S. Tedjni, "A Depolarizing Chipless RFID Tag for Robust Detection and Its FCC Compliant UWB Reading System," *IEEE Transactions on Microwave Theory and Techniques*, vol. 61, no. 8, pp. 2982–2994, Aug. 2013.

[10] L. F. Fonseca Dias, C. Jouvaud, C. Delaveaud, and H. Aubert, "Linear-to-Circular Polarization Conversion from Impedance Loading of Single-Port Patch Antennas," in *2020 IEEE International Symposium on Antennas and Propagation and North American Radio Science Meeting*, Jul. 2020, pp. 1119–1120, iSSN: 1947-1491.

[11] W. Wiesbeck and S. Riegger, "A complete error model for free space polarimetric measurements," *IEEE Transactions on Antennas and Propagation*, vol. 39, no. 8, pp. 1105–1111, Aug. 1991.

[12] D. Kahny, K. Schmitt, and W. Wiesbeck, "Calibration of bistatic polarimetric radar systems," *IEEE Transactions on Geoscience and Remote Sensing*, vol. 30, no. 5, pp. 847–852, Sep. 1992.

[13] S. H. Yueh, J. A. Kong, R. M. Barnes, and R. T. Shin, "Calibration of Polarimetric Radars Using In-scene Reflectors," *Journal of Electromagnetic Waves and Applications*, vol. 4, no. 1, pp. 27–48, Jan. 1990.

[14] R. Dybdal, "Radar cross section measurements," *Proceedings of the IEEE*, vol. 75, no. 4, pp. 498–516, Apr. 1987.

[15] C. A. Balanis, *Antenna Theory*, 3rd ed. New Jersey, USA: John Wiley & Sons, Inc., 2005.